

Transport and nonequilibrium phase transitions in polygonal urn models

Original

Transport and nonequilibrium phase transitions in polygonal urn models / Cirillo, E.N.M., Colangeli, M., Di Francesco, A., Kroger, M., Rondoni, L.. - In: CHAOS. - ISSN 1054-1500. - 32:093127(2022), pp. 1-18. [10.1063/5.0101933]

Availability:

This version is available at: 11583/2974039 since: 2022-12-21T21:24:32Z

Publisher:

American Institute of Physics (AIP)

Published

DOI:10.1063/5.0101933

Terms of use:

This article is made available under terms and conditions as specified in the corresponding bibliographic description in the repository

Publisher copyright

(Article begins on next page)

Transport and Nonequilibrium Phase Transitions in Polygonal Urn Models

Emilio N. M. Cirillo,^{1, a)} Matteo Colangeli,^{2, b)} Antonio Di Francesco,^{2, c)} Martin Kröger,^{3, d)} and Lamberto Rondoni^{4, 5, e)}

¹⁾*Dipartimento di Scienze di Base e Applicate per l'Ingegneria, Sapienza Università di Roma, via A. Scarpa 16, 00161, Roma, Italy.*

²⁾*Dipartimento di Ingegneria e Scienze dell'Informazione e Matematica, Università degli Studi dell'Aquila, via Vetoio, 67100 L'Aquila, Italy.*

³⁾*Polymer Physics, Department of Materials, ETH Zurich, 8093 Zurich, Switzerland.*

⁴⁾*Dipartimento di Scienze Matematiche, Politecnico di Torino, Corso Duca degli Abruzzi 24, 10129 Torino, Italy.*

⁵⁾*INFN, Sezione di Torino, Via P. Giuria 1, 10125 Torino, Italy.*

(Dated: 5 June 2022)

We study the deterministic dynamics of N point particles moving at constant speed in a 2D table made of two polygonal urns connected by an active rectangular channel, which applies a feedback-control on the particles, inverting the horizontal component of their velocities, when their number in the channel exceeds a fixed threshold. Such a *bounce-back* mechanism is non-dissipative: it preserves volumes in phase space. An additional passive channel closes the billiard table forming a circuit in which a stationary current may flow. Under specific constraints on the geometry and on the initial conditions, the large N limit allows nonequilibrium phase transitions between homogeneous and inhomogeneous phases. The role of ergodicity in making a probabilistic theory applicable is discussed both for rational and irrational urns. The theoretical predictions are compared with the numerical simulations results. Connections with the dynamics of feedback-controlled biological systems are highlighted.

Nonequilibrium phase transitions take place in an N -particles 2D non-dissipative billiard, constituted by two polygonal urns connected by two rectangular channels. One of the channels inverts the velocities of particles, when their number is too high, making possible a stationary inhomogeneous density distribution. A probabilistic approach is developed to predict the realization of such phenomena. Numerical simulations for irrational urns and narrow channels accurately reproduce the theoretical predictions. In that case, in fact, the billiard dynamics is expected to be ergodic, justifying the probabilistic approach. That is not the case of rational urns.

I. INTRODUCTION

The study of particle transport in confined geometries, in presence of obstacles and disorder, or of coupling with external agents concerns a large fraction of statistical mechanics literature. It has led, for instance, to understand anomalous behaviors.^{1–13} A classical example of that is afforded by single-file diffusion, that concerns particles moving in narrow channels, in which erratic motion is limited.^{14,15} Moving defects or obstacles have also been observed to sensibly affect the residence time of a particle in 1D random walks on a lattice.¹⁶ A number of variants of the Lorentz gas, such as billiards with periodically distributed flower-shaped obstacles have been devised to point out possible peculiarities of non-interacting particles transport, including the frac-

tal dependence of transport coefficients on systems parameters.¹⁷ A related research line shed light on *uphill currents* (non-Fickian currents moving *along* the density gradient), in boundary driven stochastic lattice models. Uphill currents have first been observed numerically, and also studied theoretically, in a 1D cellular automaton equipped with a long-range Kac potential.^{18–20} The hydrodynamic limit of the model was shown to correspond to a gradient flow relative to a non-local “mesoscopic” free energy functional, which generalizes the classical Ginzburg-Landau functional. The analysis was next extended to a 2D Ising model coupled to external reservoirs, where the updating rule at the boundaries is supposed to break the condition of detailed balance. The result of such nonequilibrium driving is a magnetization (uphill) current flowing from the reservoir with lower magnetization to the reservoir with higher magnetization density.^{21,22} In these models stationary uphill currents are typically sustained by first-order phase transitions, measured by an abrupt change of the order parameter, when the temperature and the magnetization of the reservoirs are carefully chosen. Similar findings have also been discussed in the context of Zero Range processes.^{23,24}

Many other works have been devoted to transport problems, but an exhaustive account is beyond the scope of our paper. Here, we focus on feedback-controlled billiard dynamics, that recently have been considered also under the point of view of finite size effects,²⁵ and of nonequilibrium phase transitions.²⁶ While the present study focuses on polygonal urns, in order to cast our results in a proper perspective, we start by reviewing the theory developed for billiards with circular urns. In particular, a system of N point particles, moving on straight lines with unit speed, and undergoing elastic collisions with the walls of a 2D billiard table different from the one studied here, has been proposed and investigated.²⁶ That table consisted of two circular urns connected by a rectangular channel, called *active* because acting as a kind of Maxwell demon that inverts the horizontal component of the particles velocities, when their number exceeds a given threshold Θ .

^{a)}E-mail: emilio.cirillo@uniroma.it

^{b)}E-mail: matteo.colangeli1@univaq.it

^{c)}E-mail: antonio.difrancesco5@graduate.univaq.it

^{d)}E-mail: mk@mat.ethz.ch

^{e)}E-mail: lamberto.rondoni@polito.it

Such a *bounce-back* mechanism, amounts to an indirect interaction between the particles, that alters the standard billiard dynamics, but preserves phase space volumes. Therefore, it can be considered formally non-dissipative. The result is a sort of rectifier, which favors a nonequilibrium phase transition with non-homogeneous stationary spatial densities. The addition of a passive channel, *i.e.* one without bounce back mechanisms, associates the nonequilibrium phase transition with a stationary current, that takes particles from the more populated urn to the other. This discharge through the passive channel establishes a stationary flow that mimics the current in a circuit generated by a battery, because in the active channel particles flow from the less to the more populated urn.²⁷

Such models have been approached in probabilistic terms, relying on the ergodicity of circular urns connected by straight channels, that holds in absence of the bounce-back mechanism.²⁸ Moreover, to make the bounce-back perturbation minimal, and the finite size effects negligible, the large N and the small channels width limit were assumed. One could then rely on a uniform distribution of particles in the billiard table, as well as on a uniform distribution of the angles of their velocities. Consistently, the earlier investigation²⁶ for equal circular urns connected by a single passive channel, or, equivalently, by an active channel with $\Theta \geq N$, showed that each particle spends, on average, the same fraction of time in each urn. Thus, a large ensemble of particles distribute themselves uniformly in such billiard tables, apart from fleeting evanescent fluctuations, that are less and less frequent as N gets larger and larger. Differently, for $\Theta < N$, ergodicity in absence of bounce-back implies that the number of particles in one gate will sooner or later exceed the threshold, activating the bounce-back mechanism. Such a feedback mechanism, which is more effective for smaller Θ and less effective for thinner channels, promotes the transition toward steady states with non-uniform mass distribution. Indeed, increasing the number of particles in one circular urn makes easier for them to crowd its gate, while particles still come from the other urn. In fact, for Θ less than a critical value (which depends on the geometrical parameters of the model), a sharp transition was observed, with a large majority of particles inside one circular urn only. Such an abrupt breaking of the left-right symmetry amounts to a nonequilibrium (first order-like) phase transition, characterized by a stationary density jump between the urns.

A difference arises between the case without passive channel and that with passive channel of finite width $w_p \neq 0$. In the first case, one circular urn gets depleted of particles, while the other urn gets more and more populated, until a steady state is reached in which the flows of particles per unit time, exchanged between the two circular urns, equalize.²⁶ In the second case, particles are able to flow between the two urns also through the passive channel, producing a net current from the more crowded to the less crowded urn.²⁷ If the ratio between channels widths w_p/w_a is large enough, this flux balances the crowding of one urn caused by the bounce-back mechanism, keeping the homogeneous state. If w_p/w_a is not large enough, an inhomogeneous state is realized.

To develop a theory of such phenomena, one question is whether ergodic properties may still be invoked, despite the

activity of the gates. Some degree of mixing should indeed allow the deterministic system to be treated like a stochastic process, and the previous works proved that such an approach provides accurate descriptions of the deterministic systems. In particular, a probabilistic framework was developed for circular urns,²⁶ that quantitatively yields the phase diagram of the homogeneous and inhomogeneous phases, as functions of the model parameters. The theoretical predictions thus obtained were confirmed by numerical simulations.

Here, we first write down the theoretical equation for the interface separating homogeneous and inhomogeneous phases in terms of a restricted set of parameters, having a clear physical interpretation. One such parameter is the threshold Θ , responsible for the bounce-back mechanism; another parameter, called λ and encoding the geometry of the system, can instead be interpreted as the typical number of particles entering a gate from the adjacent urn in the interval of time in which a particle crosses the gate. A third parameter which also appears in the interface equation corresponds to the ratio of the channel widths. We make no reference to the shape of the urns, but we trust that positions and velocities are uniformly distributed in their respective spaces. This may be imposed by hand, or be a consequence of good ergodic properties.

Therefore, we here investigate whether ergodicity of the dynamics without bounce-back mechanism is required for the phase transition to occur, considering polygonal urns whose walls make with each other angles that are irrational with respect to π , as well as urns whose sides make rational angles with each other. In fact, rational polygons are not ergodic: given the initial one, they generate only a finite number of velocities, and we analytically evaluated their number as well as their directions. The lack of ergodicity implies that the velocity distribution is anisotropic, which makes our stochastic theory not immediately applicable. Moreover, the finiteness of the number of velocities allows the identification of periodic orbits, hence of particles trapped forever in one urn. However, periodic orbits constitute a lower dimensional subset of the phase space, and are irrelevant in simulations with random initial conditions.

On the contrary, irrational polygons are expected to be ergodic. A general proof is lacking,²⁹⁻³¹ but in our case, a standard argument proves that the velocities generated from typical initial conditions are infinitely many and dense in the unit circle.

Our numerical investigation of polygonal urns will ultimately confirm that, while a nonequilibrium phase transition may take place in rational polygonal billiards, it can not be quantitatively captured by our theoretical framework, owing to the lack of ergodicity of the dynamics. Thus, the picture which emerges is that: while the microscopic origin of the phase transition can be traced back to the velocity-reversal mechanism acting in the gates, a mathematical characterization of the interface region, based on a probabilistic reasoning, can be achieved only if some sort of ergodicity holds. In fact, a related question is whether the bounce-back mechanism hinders or favours ergodicity. The present study of rational polygonal billiards will reveal that the number of velocities one particle can experience is doubled by the velocity-reversal

mechanism in the gates. Consequently, rational tables remain non-ergodic, even when the rate of activation of the bounce-back rule is high. We also show analytically that the velocity space is densely explored for our irrational polygons, in accord with Gutkin's conjecture.^{30,31}

This ultimately clarifies the nature of the bounce-back mechanism: while it is an essential ingredient in the emergence of the phase transition, it does not alter significantly the ergodic properties of the microscopic dynamics, as originally assumed. Then, the detected major discrepancies between our theory and the behavior of rational polygons, while there is perfect accord in the case of circular urns or irrational polygons, confirms that the probabilistic reasoning requires good ergodic properties. It is thus interesting to note that while transport phenomena in polygonal billiards have already been studied,^{32–37} the presence of the bounce-back mechanism constitutes a interesting novelty from the dynamical systems perspective.

Thanks to these facts, our investigation of phase transitions distinguishes between rational and irrational polygons. Furthermore, it accounts for the presence of the passive channel, see Fig. 1, which allows particles to flow freely, contrasting the trend toward inhomogeneous states.

This work is organized as follows: in Section II we describe the model by introducing the microscopic dynamics and the observables of interest. In Section III we develop the theoretical framework to characterize the phase diagram of the model. In Section IV the results of the numerical simulations are reported and compared with the theoretical predictions. Conclusions are drawn in Section V.

II. THE MODEL

Consider a billiard table Ω , made of two identical rhomboid-shaped urns, referred to as *urn 1* and *urn 2* for the left and the right urn, respectively. Each urn $U \subset \Omega$ is connected to two rectangular channels with widths w_a , w_p and lengths ℓ_a , ℓ_p , called *active* and *passive* channel. The openings of the channels are located in correspondence of the horizontal vertices of the two urns, while the longitudinal side of each channel extends along the x -axis, see Fig. 1. We also denote by ℓ_r the length of one side of the urn and by α the amplitude of the upper vertex angle. The active channel is constituted by two halves (the blue-shaded regions in Fig. 1), each of length $\ell_a/2$, called *gates*. The passive channel is also split into two halves, one located on the left of urn 1 and the other on the right of urn 2. Periodic boundary conditions are enforced along the x -direction at the leftmost and rightmost endpoints of the passive channel, thus forming a closed loop. N independent point particles move in straight lines with speed $v = 1$ inside Ω . The particles collide elastically with the boundaries $\partial\Omega$ of the table, where they undergo specular reflections.

Depending on the amplitude of the vertex angle α , the billiard table is classified as a *rational* polygon, if $\alpha/\pi = p/q$ with $p, q \in \mathbb{N}$, or an *irrational* polygon, if α is not a rational

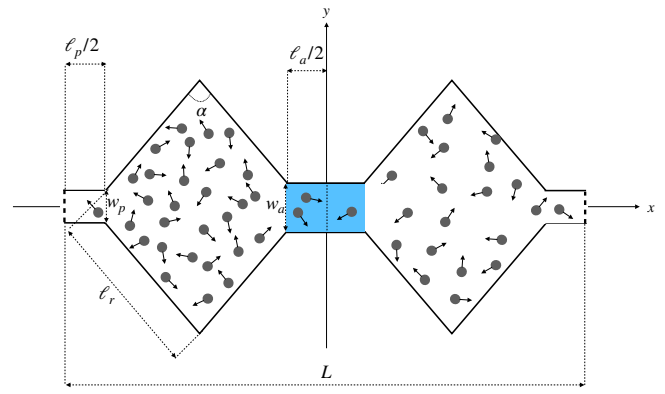


FIG. 1. The billiard table: N point particles are represented as small disks, their velocities are represented by arrows. Shown are the two polygonal urns connected by two rectangular channels (periodic boundary conditions are imposed at the leftmost and rightmost ends of the table, displayed as thick dashed lines). The two blue-shaded regions inside the active channel, are the two gates in which the bounce-back mechanism separately acts. The horizontal component of the velocity of the particles contained in one gate and moving toward the other is reversed whenever their number is larger than the threshold Θ . Rational and irrational urns refer to the value of α/π .

multiple of π . Such distinction is of paramount importance in establishing the ergodic properties of the dynamics in polygonal billiards which to date is, in general, an open problem.^{30,31}

What distinguishes our model from a standard billiard is a dynamical rule, characterizing the dynamics in the two gates of the active channel, originally introduced in Ref.²⁶: the *bounce-back* mechanism. Such rule works as follows: when the number of particles in one gate, which are moving toward the other gate, exceeds a fixed threshold Θ , the horizontal component of their velocity is reversed. Particles in a gate which are coming from the other gate are not affected by the mechanism, and may continue their motion unaltered.

A quantitative study of the phase transition in our model starts with the definition of a suitable order parameter. To this aim, we introduce the observable called *mass spread*, defined as:

$$\chi(t) := \frac{N_2(t) - N_1(t)}{N}, \quad (1)$$

where $N_1(t)$, $N_2(t)$ denote the (instantaneous) number of particles residing in urn 1 and urn 2, respectively, at time t . We then compute the absolute value of the time averaged mass spread, $\bar{\chi}$, viz.:

$$\bar{\chi} := \left| \frac{1}{T} \int_0^T \chi(t) dt \right|. \quad (2)$$

with T large enough, to ensure that the time average attains an asymptotic value. The observed steady states are thus described by different values of $\bar{\chi}$: while homogeneous states correspond to $\bar{\chi} = 0$, $\bar{\chi}$ close to 1 refers to unequal distribution of particles in the urns.

Another important observable is the particle current, which is defined as follows. Let $x = 0$ be the position of the vertical

line separating the two gates of the active channel and consider a long time interval $[0, T]$. Denote by $\Delta n(T)$ the number of particles that in the time $T \gg 1$ cross $x = 0$ in the direction from urn 1 to urn 2 minus those moving in the opposite direction. Then, the net stationary current *per particle* is defined by:

$$\bar{J} := \frac{\Delta n(T)}{NT} \quad (3)$$

Before proceeding further with the theoretical description of the model, in the remainder of this Section we shall focus on some ergodic properties of the billiard models considered in this work. We shall restrict our discussion for a moment to closed rhomboid-shaped polygons, *i.e.* urns with $w_a = w_p = 0$. Let θ_0 be the direction of the velocity of a particle at time 0 with respect to the positive direction of the horizontal axis, and θ_k the corresponding direction after k collisions. The sequence of velocities fully specified by $(\theta_k)_{k \in \mathbb{N}}$ is obtained from the mapping $M_\alpha : [0, 2\pi] \times \{-1, +1\} \rightarrow [0, 2\pi]$ defined as:

$$\begin{aligned} \theta_k &= M_\alpha(\theta_{k-1}, \sigma_k) \\ &= \pi + \sigma_k \alpha - \theta_{k-1} \pmod{2\pi}, \end{aligned} \quad (4)$$

where the sign $\sigma_k \in \{-1, +1\}$ is determined by the position of the reflection point on the surface of the urn: $\sigma_k = +1$ for the opposing top right and bottom left sides of the urn, and $\sigma_k = -1$ for the remaining two sides. It is important to apply the modulus in Eq. (4) at each iteration, and not only once after k iterations. A natural question thus regards the characterization of the allowed velocity directions in the urn. It turns out that for irrational polygons (α/π is an irrational number), θ densely covers the whole set $[0, 2\pi]$. This is immediately seen from Eq. (4): the map M_α generates an irrational rotation on the circle $\mathbb{R}/(2\pi\mathbb{Z})$, hence orbits are dense in $[0, 2\pi]$. This leads to a uniform exploration of the billiard table, meaning that sets of equal area are visited with equal frequency. However, the rate at which such a uniform distribution is reached sensibly depends on θ_0 , cf. Fig. 2 for the rate at which the interval $[0, 2\pi]$ is explored starting from different initial velocity angle θ_0 .

Instead, for rational polygons (*i.e.*, if $\alpha/\pi = p/q$, with p, q some integer numbers), the angle θ takes up just a finite number of values. In fact, for a given θ_0 , there are at most $2q$ admissible velocity directions, and exactly $2q$ different directions if θ_0 is irrational. Specifically, if q is odd,

$$\theta \in \left\{ \frac{2n\pi}{q} \pm \theta_0 \right\}_{n \in \{1, 2, \dots, q\}} \pmod{2\pi} \quad (5)$$

holds, whereas taking even q in Eq. (4) yields

$$\theta \in \left\{ \frac{2n\pi}{q} + \theta_0, \frac{(2n+1)\pi}{q} - \theta_0 \right\}_{n \in \{1, 2, \dots, q\}} \pmod{2\pi} \quad (6)$$

For instance, for a closed rational urn with $\theta_0 = \pi/\sqrt{3}$, which is irrational, Eq. (5) evaluates to

$$\theta \in \{\theta_0, 2\alpha \pm \theta_0, 4\alpha \pm \theta_0, 6\alpha - \theta_0\} \quad (7)$$

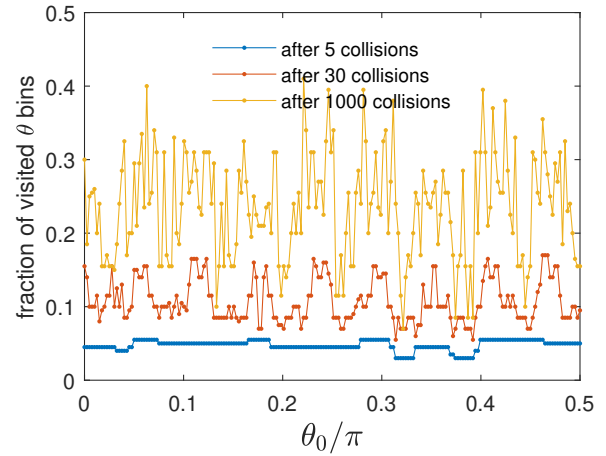


FIG. 2. Fraction of visited θ bins (velocity angle intervals) for the closed irrational rhombic urns with vertex angle $\alpha = \pi/\sqrt{8}$, as function of the initial velocity direction $\theta_0 \in [0, \pi/2]$. To obtain a single point in this graph, $N = 10^{15}$ particles are initially distributed homogeneously inside the urn, the initial velocities are uni-directional with angle θ_0 ; for symmetry reasons results depend only on $|\cos \theta_0|$. The bin size is $\pi/200$, *i.e.*, the interval $[0, \pi/2]$ is divided into 100 bins. The result is independent on N for sufficiently large N , as the same result is obtained integrating instead of summing over particles.

for $\alpha = \pi/3$ (odd q), while Eq. (6) produces

$$\theta \in \{\theta_0, 2\alpha + \theta_0, 3\alpha - \theta_0, 5\alpha - \theta_0\} \quad (8)$$

for $\alpha = \pi/2$ (even q), which is also shown by our numerical simulations (see Figs. 6 and 13 below).

In the presence of the active channel ($w_a > 0$), a velocity reversal in x -direction corresponds to $\sigma_k = 0$ in Eq. (4). This may lead to additional members in the set of possible θ values. For the case of Eq. (7), the additional six angles are given by:

$$\theta \in \{\pm\alpha + \theta_0, 3\alpha \pm \theta_0, 5\alpha - \theta_0, 7\alpha - \theta_0\} \quad (9)$$

while for the case of Eq. (8), there are no additional angles, in agreement with numerical results to be presented below. Note that for rational polygons with rational θ_0 the above general expressions still apply, but the number of different θ is eventually reduced; repeated entries have to be ignored from the list of size $2q$. For example, for rational $\theta_0 = \alpha/2$, every entry in the list appears twice, and there are only q different θ 's.

III. THEORY

In this section, following ideas developed earlier,^{26,27} we outline briefly the theoretical framework describing the phase transition in the system. A key ingredient in our derivation is the single-particle invariant probability density $\rho(\mathbf{x}, \mathbf{v})$ to find one particle at $\mathbf{x} \in U$ with velocity $\mathbf{v} = (v \cos \theta, v \sin \theta)$, where the speed $v > 0$ is fixed. Our derivation is based on the assumption that the presence of the rectangular channels does not alter significantly the ergodic properties of the dynamics in the closed rhomboidal urns. Furthermore, given that

the dynamics preserve phase space volumes, we postulate that $\rho(\mathbf{x}, \mathbf{v})$ is uniform in U and on the interval $[0, 2\pi]$. It can thus be written as $\rho = (2\pi A)^{-1}$, with

$$A = \ell_r^2 \sin \alpha - \frac{w_a^2 + w_p^2}{4} \tan\left(\frac{\alpha}{2}\right) \quad (10)$$

the area of a single rhomboid-like urn. While the assumption about the uniformity of the density seems appropriate for irrational polygons, it is unjustified for rational polygons, in which only few velocity directions are in fact admitted. We may hence expect our theory to capture the phase transition more appropriately with irrational than with rational polygons: this will indeed be confirmed by our numerical investigation, in Section IV. Let us call

$$\bar{N}_i := \frac{1}{T} \int_0^T N_i(t) dt, \quad i \in \{1, 2\} \quad (11)$$

the stationary number of particles in the i -th urn ($T \gg 1$, as in Eq. (2) and τ_a (resp. τ_p) the typical time needed for a particle to cross one gate in the active (resp. passive) channel.

Owing to the uniformity of the density $\rho(\mathbf{x}, \mathbf{v})$ (in the simulations, this requires large N , otherwise unoccupied regions that defeat uniformity are necessarily too large), expressions can be derived for the stationary current flowing through the active and passive channels (details are given in the Appendix A). They are determined by $\lambda_{i,a}$ (or $\lambda_{i,p}$) that can be interpreted as the typical number of particles which, in the time interval τ_a (or τ_p), enter the active (or passive) gate from the adjacent i -th urn. We find

$$\lambda_{i,a} = \bar{N}_i \frac{w_a \ell_a}{4A}, \quad \lambda_{i,p} = \bar{N}_i \frac{w_p \ell_p}{4A}, \quad (12)$$

for $i \in \{1, 2\}$, and

$$\tau_a = \frac{\pi \ell_a}{4v}, \quad \tau_p = \frac{\pi \ell_p}{4v}. \quad (13)$$

For the current flowing through the passive channel we obtain in terms of these quantities

$$\bar{J}_p(t) = \frac{1}{N\tau_p} (\lambda_{2,p} - \lambda_{1,p}). \quad (14)$$

The current flowing through the active channel is instead reduced by the action of the bounce-back mechanism in the gates, and attains the modified form

$$\bar{J}_a(t) = \frac{1}{N\tau_a} \left[\frac{\lambda_{1,a}\Gamma(\Theta, \lambda_{1,a}) - \lambda_{2,a}\Gamma(\Theta, \lambda_{2,a})}{\Gamma(\Theta)} \right], \quad (15)$$

where $\Gamma(y, x)$ is the Euler upper incomplete gamma function defined in Eq. (A6), and $\Gamma(y) = \Gamma(y, 0)$.

The current \bar{J}_a is conventionally taken as positive if the flow goes from the left to the right urn through the active channel. Analogously, \bar{J}_p is conventionally taken as positive if the flow goes from the right to the left urn through the passive channel (periodic boundary conditions are imposed).

The condition of stationarity requires the equality of the currents \bar{J}_a and \bar{J}_p in Eqs. (14) and (15). Therefore, letting $\eta := N\tau_a(\bar{J}_a - \bar{J}_p)$, one has

$$\eta = \lambda_{1,a} \frac{\Gamma(\Theta, \lambda_{1,a})}{\Gamma(\Theta)} - \lambda_{2,a} \frac{\Gamma(\Theta, \lambda_{2,a})}{\Gamma(\Theta)} - \frac{\tau_a}{\tau_p} (\lambda_{2,p} - \lambda_{1,p}). \quad (16)$$

Using the definitions (12), one has $\lambda_{i,p} = \lambda_{i,a} w_p \ell_p / w_a \ell_a$, and noting that $\tau_a / \tau_p = \ell_a / \ell_p$, Eq. (16) can thus be written as

$$\eta = \lambda_{1,a} \left[\frac{\Gamma(\Theta, \lambda_{1,a})}{\Gamma(\Theta)} + \frac{w_p}{w_a} \right] - \lambda_{2,a} \left[\frac{\Gamma(\Theta, \lambda_{2,a})}{\Gamma(\Theta)} + \frac{w_p}{w_a} \right] = 0. \quad (17)$$

Note that here the ratio w_p/w_a can be taken as a single parameter. That is also possible because our results can be scaled and we choose a length unit so that $w_a = 1$. However, in the following, we continue writing w_p/w_a to highlight its meaning as a ratio of widths.

When most of the particles reside inside the urns, *e.g.* in the case $N_1, N_2 \gg \Theta$, we have $N \approx \bar{N}_1 + \bar{N}_2$, and the typical number of particles entering the active channel from both urns, in a time $\tau_a/2$,

$$\lambda := N \frac{w_a \ell_a}{8A} \quad (18)$$

obeys $\lambda = (\lambda_{1,a} + \lambda_{2,a})/2$. Consequently, $\lambda_{2,a} = 2\lambda - \lambda_{1,a}$, and the stationary mass spread is given by:

$$\bar{\chi} = \frac{|\lambda_{2,a} - \lambda_{1,a}|}{\lambda}. \quad (19)$$

The existence of multiple solutions of Eq. (17) signals the onset of a phase transition. One solution, as it can be easily verified by direct inspection, is $\lambda_{2,a} = \lambda$, or equivalently, $\bar{N}_2 = N/2$, which corresponds to the equilibrium state $\bar{\chi} = 0$. More solutions may appear, though, which bring the stationary dynamics out of equilibrium. Indeed, as shown in Figs. 3 and 4, for certain parameters values, η changes sign in intervals not containing $\lambda_{2,a} = \lambda$. The roots in these intervals correspond to nonequilibrium states, $\bar{\chi} > 0$. Given the differentiability of η , one may ask which of the steady states is stable, when η vanishes more than once for $\lambda_{2,a} \in [\lambda, 2\lambda]$.

The linear stability analysis states that a stationary state is stable if $(\partial\eta/\partial\lambda_{2,a}) \leq 0$, otherwise it is unstable^{26,27}. Hence, the theoretical transition line between homogeneous and inhomogeneous phases is identified by the locus of points at which

$$\left. \frac{\partial\eta}{\partial\lambda_{2,a}} \right|_{\lambda_{2,a}=\lambda} = 0. \quad (20)$$

Using Eqs. (17) and (18), the condition (20) becomes

$$\left. \frac{\partial\eta}{\partial\lambda_{2,a}} \right|_{\lambda_{2,a}=\lambda} = 2 \left[\frac{\lambda^\Theta e^{-\lambda} - \Gamma(\Theta, \lambda)}{\Gamma(\Theta)} - \frac{w_p}{w_a} \right] = 0, \quad (21)$$

or, equivalently,

$$\frac{\lambda^\Theta e^{-\lambda}}{\Gamma(\Theta)} - \frac{\Gamma(\Theta, \lambda)}{\Gamma(\Theta)} = \frac{w_p}{w_a}. \quad (22)$$

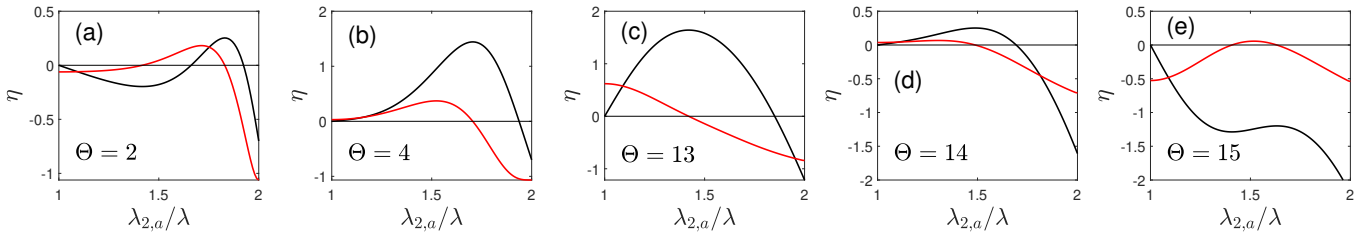


FIG. 3. Plots of η (black solid line) and $\partial\eta/\partial\lambda_{2,a}$ (red solid line) at fixed $N = 1000$ and fixed geometry as functions of the normalized variable $\lambda_{2,a}/\lambda$, for $\ell_a = 1.0$, $\ell_r = 2$, $\alpha = \pi/\sqrt{8}$, and $w_a = 0.3$, $w_p = 0.01$, hence $w_p/w_a > 0$, $\lambda \approx 10.5$ and $A \approx 3.57$. Zeroes of the black curve identify stationary states. Panel (a), $\Theta = 2$: homogeneous linearly stable state with no current; moderately inhomogeneous unstable state with current; strongly inhomogeneous linearly stable state with current. Panels (b,c,d), $\Theta = 4, 13, 14$: homogeneous unstable state; inhomogeneous linearly stable state with current. Panel (e), $\Theta = 15$: linearly stable homogeneous state, with no current.

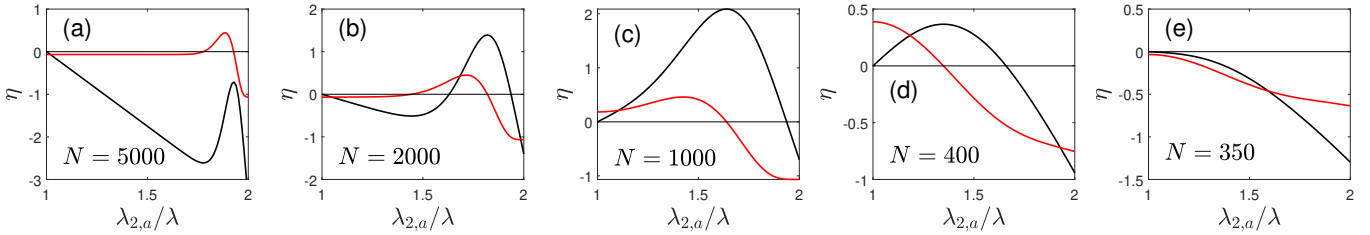


FIG. 4. Plots of η (black solid line) and $\partial\eta/\partial\lambda_{2,a}$ (red solid line) at fixed $\Theta = 5$ and fixed geometry (same as in Fig. 3) as functions of the normalized variable $\lambda_{2,a}/\lambda$. Zeroes of the black curve identify stationary states. Panel (a), $N = 5000$: homogeneous linearly stable state with no current. (b), $N = 2000$: three steady states: homogeneous linearly stable state with no current, moderately inhomogeneous linearly stable state with current, strongly inhomogeneous linearly stable state with current. Panels (c,d), $N = 1000, 400$: homogeneous unstable state and inhomogeneous linearly stable state with current. Panel (e), $N = 350$: linearly stable homogeneous state, with no current.

Equation (22) is a central result of our theoretical derivation, as it yields the behavior of the system determined by the parameters Θ , λ and w_p/w_a . It holds not only for polygonal urns but also for circular urns, if A is the area of a circular urn. Note that most (all for $w_p = 0$) geometric parameters determining the shape of the billiard table, ℓ_r , ℓ_a , α , w_a and w_p directly contribute to the value of λ . Then, fixing the ratio w_p/w_a in Eq. (22), one obtains the equation $\lambda = \lambda(\Theta)$ for the line delimiting the different phases.

For $w_p/w_a = 0$, Eq. (22) has a single solution separating the only two stationary states that exist when the passive channel is absent: the homogeneous state ($\bar{\chi} = 0$) and the totally inhomogeneous state ($\bar{\chi} = 1$).

For positive but sufficiently small w_p/w_a , the line $\lambda = \lambda(\Theta)$ turns concave with a maximum at $\lambda = \Theta + 1$. Then, Eq. (22) has two solutions in the interval $[\lambda, 2\lambda]$, that represent the two interfaces $\lambda_+(\Theta)$, $\lambda_-(\Theta)$ which split the parameter space into three regions. The first, also occurring in the single channel model, corresponds to the homogeneous state in which the bounce-back is in-effective. The second corresponds to an inhomogeneous state, $0 < \bar{\chi} < 1$, and a steady current in the circuit. In this case, a net current from the more to the less populated urn flows through the passive channel, while the active channel plays the role of an *efm*, that maintains a kind of *potential difference*, allowing more particles to go from the less populated urn to the more populated urn, than vice-versa. The third region, characterized by $\bar{\chi} = 0$, corresponds to a situation in which the particles exiting the urns through the

passive channel are not efficiently replaced by those bouncing back in the active channel. The state is homogeneous and no net current is produced.

It is finally interesting to note that a stable homogeneous and a stable inhomogeneous state may coexist, as shown in Fig. 3(a), where two inhomogeneous stationary states appear: one is unstable and the other one is stable. The theoretically predicted behavior of $\bar{\chi}$ is reported in the plots in Fig. 5, whereas numerical evidence of the coexistence of homogeneous and inhomogeneous states will be shown below in Fig. 9.

In the next Section we will compare our theory with the results of the numerical simulations of the dynamics. The comparison will enable us to reveal the role of the ergodicity of the dynamics in our theory of nonequilibrium phase transitions, since that depends on the geometry.

IV. SIMULATION RESULTS

The theoretical analysis of the stationary behavior of the model, developed in Section III, is complemented here with a detailed computational study of the dynamics inside the table Ω , that does not rely on the assumptions of the theory. A bounce-back event-driven algorithm has been implemented to evolve the particles trajectories basically independently, at asynchrone time steps, to allow for maximum execution speed. Each particle propagates directly, from its cur-

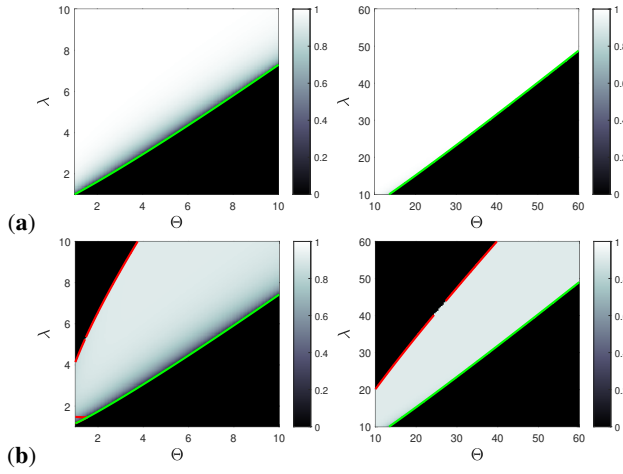


FIG. 5. Stationary mass spread $\bar{\chi}$ as a function of the variables λ and Θ for two different values of the ratio w_p/w_a , (a) $w_p/w_a = 0$ and (b) $w_p/w_a = 0.05$, computed through formula (19). Left panels show the plots in the range $\lambda, \Theta \in [1, 10]$, while right panels show zoomed out plots for the larger range $\lambda, \Theta \in [10, 60]$, with $N = 10^3$. The green and red solid lines represent the one or two solutions of the interface equation (22), delimiting the different phases, the different stationary states, corresponding to different $\bar{\chi}$.

rent position, to the time and position where it enters or exits a gate of the active channel. Not only is the period of time thus a variable for each particle, but also the number of its collisions with the system walls until it reaches or exists a gate (a much more time-consuming but simpler implementation runs at identical time step for all particles, at a variable time step that corresponds to the shortest time until next collision; less efficient implementations exist as well). Entrance and exit times for each single particle are recorded and analyzed; whenever the number of detected particles contemporary spending time in one of the gates exceeds the threshold Θ , their trajectory is rewinded and the horizontal component of the velocity of those occupying the gate is reversed. This way the bounce-back mechanism is implemented exactly. A steady state detection procedure is implemented, based on the constantly recorded value of $\chi(t)$; in particular, the beginning of the averaging period is defined as the time instant t at which the distance $||\chi(t) - \chi(0)||$ has reached its all time maximum value. Because $\chi(t)$ tends to approach a stationary value within fluctuations, the whole averaging period is considered to represent the steady state. Once the steady state is detected, the simulation evolves the dynamics for an adjustable amount T of time, according to the desired accuracy of the averaging procedures.

In each set of simulations, the number of simulated particles N is fixed, while the geometrical features of the billiard table (i.e., ℓ_r and α for the urns, w_a , w_p , ℓ_a and ℓ_p for the active and passive channels) and the threshold value Θ are adjusted to explore the parameter space. We are going to present results for the initial state, where all particles reside in one of the urns, $\chi(0) = 1$. This choice is computationally advantageous, as the regime of large λ and small Θ , for which $\bar{\chi} = 1$ is the usual scenario, is otherwise only reached at enormous

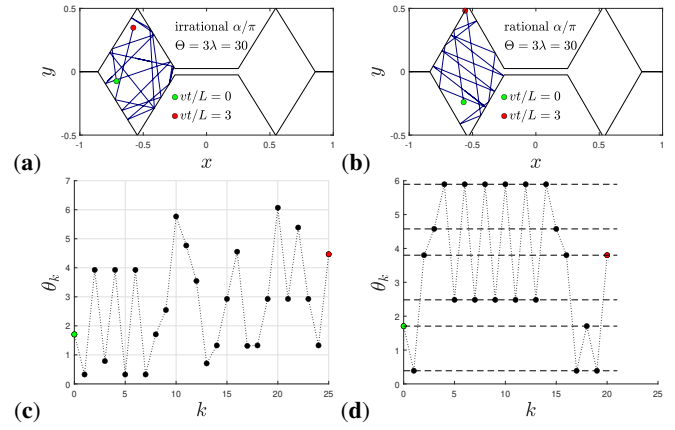


FIG. 6. Short trajectory of a tagged particle inside the billiard table with $w_p/w_a = 0.05$, and unidirectional initial velocities with direction $\theta_0 = \pi/\sqrt{3}$. (a): orbits of irrational polygon with $\alpha = \pi/\sqrt{8}$; (b) orbits of rational polygon with $\alpha = \pi/3$. Panels (c) and (d) show the corresponding directions θ_k of the velocity after the k -th collision. Dashed horizontal lines in (d) mark the expected discrete values known from Eq. (7). Parameters are set to $\lambda = 10$, $\Theta = 30$, $w_a = 0.05$, $\ell_a = 0.5$, $\ell_p = 0.5$, $N = 10^3$, with L the total horizontal length of the billiard table, cf. Fig. 1.

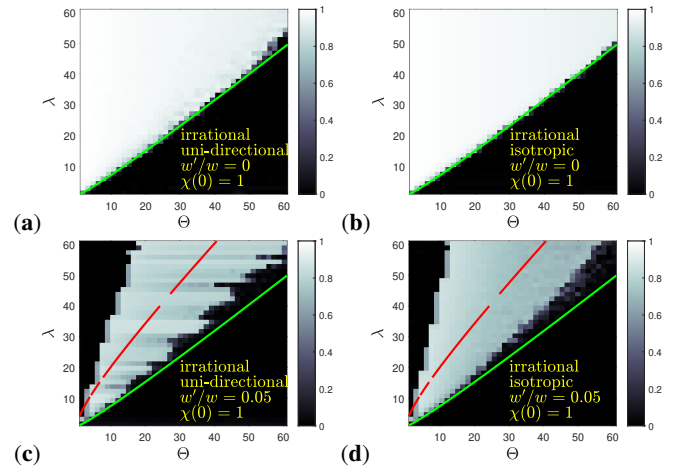


FIG. 7. Mass spread $\bar{\chi}$ as a function of λ and Θ for an irrational polygon with $\alpha = \pi/\sqrt{8}$. Red and green solid lines denote the numerical solution to the interface equation (22) with (a,b) $w_p/w_a = 0$ and (c,d) $w_p/w_a = 0.05$, respectively. Plots on the two left panels (a,c) refer to uniform initial distribution of velocities, plots (b,d) on the right refer to unidirectional initial velocities, all pointing along the direction $\theta_0 = \pi/\sqrt{3}$. Differences are minimal and of merely statistical nature. Other parameters are: $w_a = 0.05$, $\ell_a = 0.5$, $\ell_p = 0.5$, $N = 10^3$ (same as in Fig. 6).

computational effort. We have paradigmatically verified that results are insensitive to the choice of $\chi(0)$.

Note that the system parameters can be limited to λ , Θ and w_p/w_a , since they determine the stationary properties of the dynamics, via Eq. (17). Thus, the assumption that $N_1 + N_2 \approx N$ in the limit of small channels, and Eq. (12), imply that the length ℓ_p of the passive channel does not belong to the set of parameters to be explored. Nevertheless, we remark

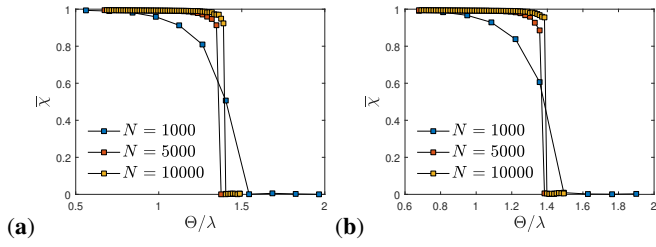


FIG. 8. Behavior of $\bar{\chi}$ as a function of Θ/λ for $N = 10^3$, 5×10^3 , and 10^4 , with $\ell_r = 0.7$, $w_a = 0.05$, $w_p = 0$, $\ell_a = 0.5$ for: (a) irrational $\alpha = \pi/\sqrt{8}$, and (b) rational $\alpha = \pi/3$ urns. Initial velocities are isotropic. For (a) $\lambda = 0.00712394 \times N$, hence $\Theta/\lambda \approx 1.371$ ($N = 1000$), 1.255 ($N = 5000$), and 1.2016 ($N = 10000$), while for (b) $\lambda = 0.00737043 \times N$, hence $\Theta/\lambda \approx 1.3703$ ($N = 1000$), 1.2509 ($N = 5000$), and 1.1993 ($N = 10000$), cf. interface Eq. (22).

that the magnitude of ℓ_p may affect the simulation times and must also be properly tuned in order to meet the assumptions introduced by the theory. The results are presented in two different subsections: the first shows simulations results for irrational polygon with vertex angle $\alpha = \pi/\sqrt{8}$, while the second refers to a rational polygonal table with $\alpha = \pi/3$. For both set-ups, two different initial distributions of particles velocities are tested, corresponding to random uniformly distributed initial velocities and to unidirectional initial velocities pointing along the direction θ_0 . Sample trajectories starting from $\theta_0 = \pi/\sqrt{3}$, for the two set-ups with irrational and rational polygonal urns, are illustrated in panels (a) and (b) of Fig. 6. Panel (d) of the same figure shows that, in the case of rational polygonal urn with $\alpha = \pi/3$, the values of the velocity directions after the k -th collision on the walls, identified by the angle θ_k , match the finite set of values predicted by Eq. (7). Instead, in the case of an irrational polygonal urn with $\alpha = \pi/\sqrt{8}$, the values of θ_k tend to fill up densely the interval $[0, 2\pi]$, as evidenced in panel (c).

A. Irrational Polygon

Here we report the results from simulations of the irrational polygon described above. Figure 7 shows the steady state mass spread $\bar{\chi}$ as function of the parameters λ and Θ , for different values of the ratio w_p/w_a .

As the plots show for both types of initial conditions, the case with a single active channel (i.e. $w_p = 0$) behaves as theoretically expected: the inhomogeneous steady state with $\bar{\chi} = 1$ is confined in the parameters space region predicted by the theory. The correspondence with the solution of the interface equation is perfect, which validates also the ergodic hypothesis underlying our reasoning. The same can not be directly said about the configurations with $w_p \neq 0$. For instance, taking $w_p/w_a = 0.05$, none of the initial conditions of velocities seems to precisely drive the system towards the expected behavior. The agreement between theory and simulations, cf. the lower green transition line in the bottom panels of Fig. 7, is better realized at small values of λ , namely when the rhomboidal geometry of the urns is not significantly affected by the

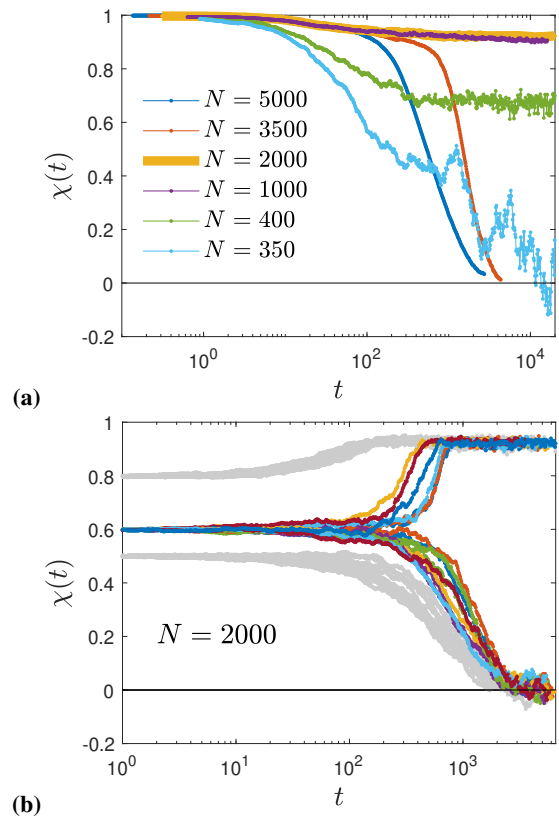


FIG. 9. Dynamical behavior of $\chi(t)$ as a function of time for various N at $\Theta = 5$ and same geometry as in Fig. 4, supplemented by $\ell_p = \ell_a$. Initial velocities are randomly oriented. (a) Initial state obeys $\chi(0) = 1$. To limit the noise and highlight the trends, all curves represent averages over 20 independent trajectories. The behavior approximates for growing N the theoretical one represented in Fig. 4: for small N , $\chi(t)$ rapidly vanishes; for larger N , $\chi(t)$ remains longer close to 1, till its decay to 0 takes too long to be observed. (b) $N = 2000$. $\chi(0) = 0.6$ is at the boundary of the region attracted by the homogeneous state and the one asymptotically in N attracted by the inhomogeneous stable state. For $\chi(0) > 0.6$, $\chi(t)$ increases toward the inhomogeneous stable value. For $\chi(0) < 0.6$, $\chi(t)$ goes to 0.

presence of the channels. However, also this is in accord with our theoretical derivations, which assume the channels negligible in size, so the standard billiard dynamics be only weakly altered.

The dependence of $\bar{\chi}$ on N , when the geometrical parameters are fixed, is shown in panel (a) of Fig. 8. The plot gives $\bar{\chi}$ as a function Θ/λ for different values of N : an increase of N makes the transition region sharper and sharper, thus resembling the classical behavior observed in first-order phase transitions in the large N limit. In fact, this limit is necessary also for the stability of the theoretically predicted inhomogeneous stationary states, because, at finite N , only the homogeneous state is stable. The reason is that the homogeneous state occupies by far the largest fraction of the phase space and ergodicity implies that sooner or later it is achieved. However, fluctuations away from equilibrium are possible at finite N , and last longer and longer as N grows. This does not contra-

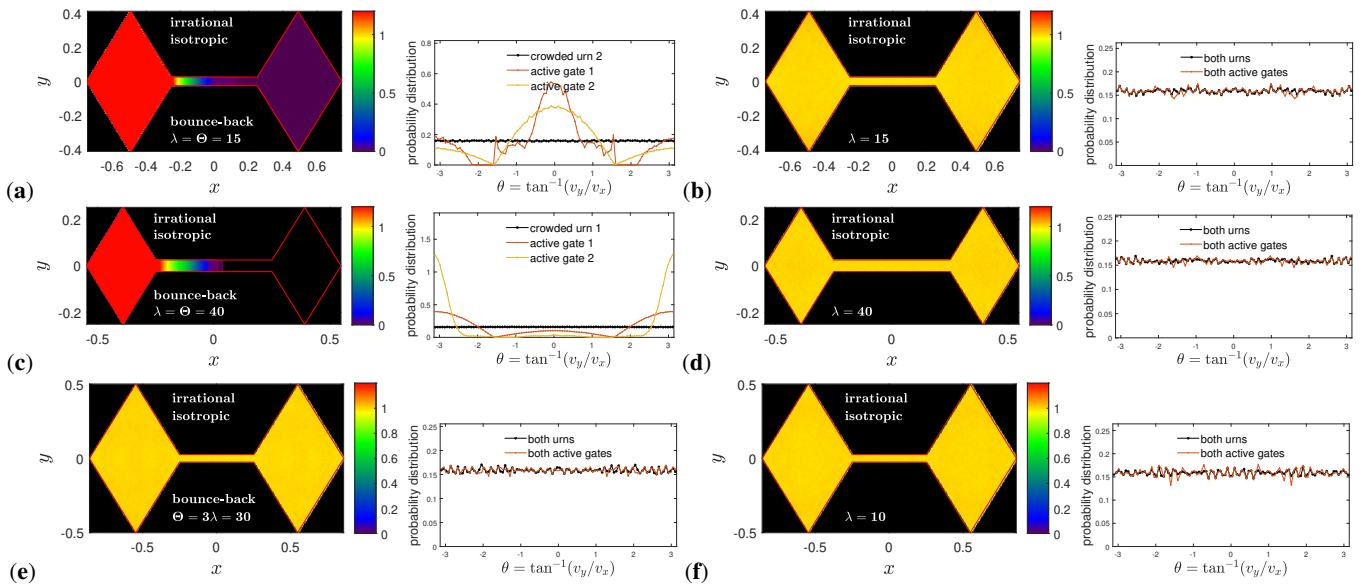


FIG. 10. Irrational polygons with $\alpha = \pi/\sqrt{8}$, connected by a single channel. Initial velocities are randomly distributed. In (a,c,e) the channel is active; in (b,d,f) it is not. Each panel shows a stationary density plot, normalized by the mean density, and the corresponding stationary velocity histogram. (a,b) $\lambda = \Theta = 15$, (c,d) $\lambda = \Theta = 40$, and (e,f) $\lambda = 10$, $\Theta = 30$. Remaining parameters are: $w_a = 0.05$, $\ell_a = 0.5$, $\ell_p = 0.5$, $N = 10^3$ (same as in Fig. 6).

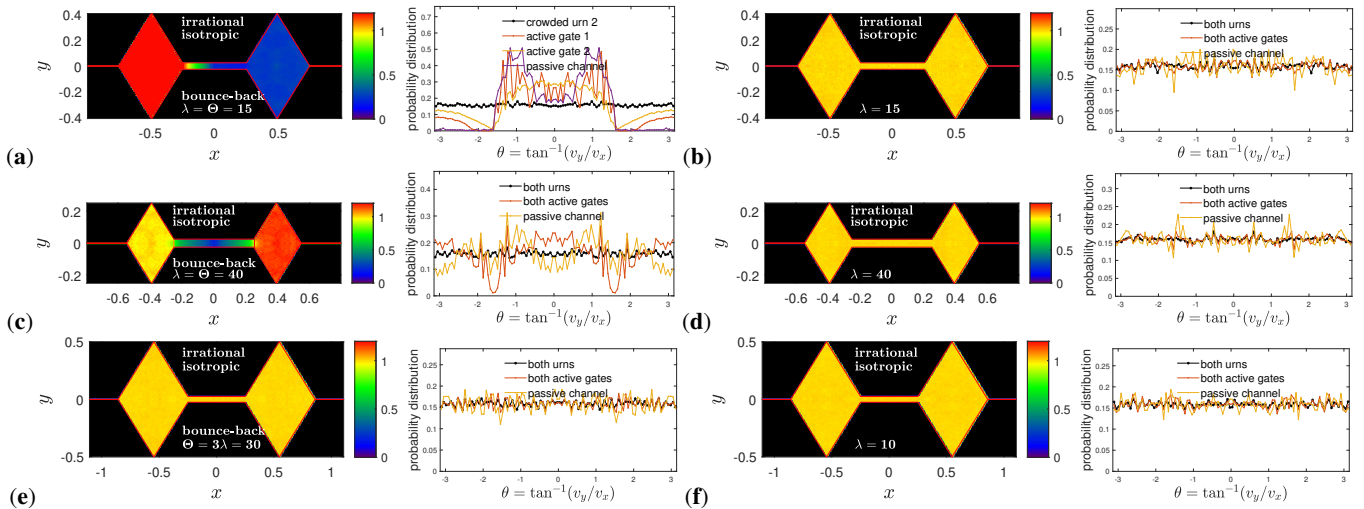


FIG. 11. Irrational polygons with $\alpha = \pi/\sqrt{8}$, connected by active and passive channels, with $w_p/w_a = 0.05$. Initial velocities are randomly distributed. In panels (a,c,e) the bounce-back mechanism is at work; in panels (b,d,f) it is not. Each panel shows a reduced stationary density plot and the corresponding stationary velocity histogram. (a): $\lambda = \Theta = 15$; (b) λ like (a). (c) $\lambda = \Theta = 40$ (d) λ like (c). (e) $\lambda = 10$, $\Theta = 30$, (f) λ like (e). Remaining parameters are: $w_a = 0.05$, $\ell_a = 0.5$, $\ell_p = 0.5$, $N = 10^3$ (same as in Fig. 6).

dict Figs. 3 and 4, since they are based on a stochastic theory that assumes a uniform distribution in positions and velocities. Hence it applies only to systems made of many particles, and turns more accurate for larger N , if particles are randomly distributed. Indeed, Fig. 9 shows how inhomogeneous states considered stable by the stochastic theory turn from unstable to stable as N grows, and within the range of N values in which they exist (changing N with other parameters fixed may change the number of steady states), cf. Fig. 4. The same holds for circular urns.

Letting $\mathcal{A} = 2A + \ell_a w_a + \ell_p w_p$ be the total area of the billiard table, and N/\mathcal{A} the mean particle number density, Figs. 10 and 11 display the reduced stationary particle density profiles, i.e., local number density multiplied by \mathcal{A}/N , and the velocity profiles in the urns and in the channels, in presence (panels (a), (c), (e)), and in absence (panels (b), (d), (f)) of the bounce back mechanism. For different values of the parameters (Θ, λ) at $w_p/w_a = 0$ and at $w_p/w_a = 0.05$, a comparison of panels (a) and (b), as well as of panels (c) and (d) of Fig. 10, shows that a uniform distribution of particles is always

obtained in absence of bounce-back, but even in presence of bounce-back events, the distribution can be uniform, if λ and Θ are properly tuned. Furthermore, the histograms of the velocities in the urns are uniform in $[0, 2\pi]$, as required for the application of the probabilistic method of Section III. As discussed in Section II, this owes to the fact that the map M_α in Eq. (4) is ergodic for irrational polygonal urns. When the bounce-back mechanism is efficiently at work, and produces a phase transition, the distribution of velocities in the channels is naturally altered.

An analogous numerical investigation has been carried out also for irrational polygonal billiards equipped with a passive channel, with $w_p/w_a = 0.05$. In this case, a stationary current may be established in the circuit constituted by urns and channels, with the active channel acting as an *emf*. Our simulations show that both the density and the velocity histograms referring to the crowded urn (for which a meaningful statistics is available) remain approximately uniform, even in presence of a stationary current, cf. Fig. 11.

B. Rational Polygon

Here, we report our results, obtained from simulations of rational polygons dynamics. Figure 12 shows the steady state mass spread $\bar{\chi}$ as a function of the normalized parameters λ/N and Θ/N , for different values of the ratio w_p/w_a with $\alpha = \pi/3$. Left and right panels in the figure refer to unidirectional initial velocities and random initial velocities, respectively; top and bottom panels refer to tables with $w_p/w_a = 0$ and $w_p/w_a = 0.05$, respectively. Unlike the irrational case, our rational case with $w_p = 0$ matches the theoretical predictions only when a uniform initial velocity distribution is simulated, cf. panel (b) in Fig. 12. Indeed, as mentioned in Section II the map M_α in Eq. (4) is non-ergodic for rational rhomboidal urns. However, as revealed by panels (b) and (d), that difficulty for the application of our theory, which assumes that all velocities are available, is overcome if the initial distribution of velocities is random and N is large. Deviations from the theoretical predictions are instead visible in panel (a) of Fig. 12, and become even more severe in panel (c), where the phase transition foreseen by the theory is not even detected. This result clarifies further the role of ergodicity, and of the bounce-back mechanism. Despite being a key ingredient, the bounce-back does not suffice, *per se*, to produce the phase transition, for some degree of uniformity of the velocity distribution is also required.

As also observed with irrational urns, the addition of the passive channel, which may give rise to a stationary current flowing through the billiard table, leads in panel (d) of Fig. 12 to some tiny deviations from the theoretical lower interface lines at large values of λ and Θ .

Figures 13 and 14 confirm the presence of a finite number of velocities in the steady state dynamics: the position of the peaks is well described by the formula given in Eq. (7), as also seen in panel (c) of Fig. 6. An inspection of the velocity histograms in the left and the right columns of both figures also highlights the role of the bounce-back mechanism in doubling

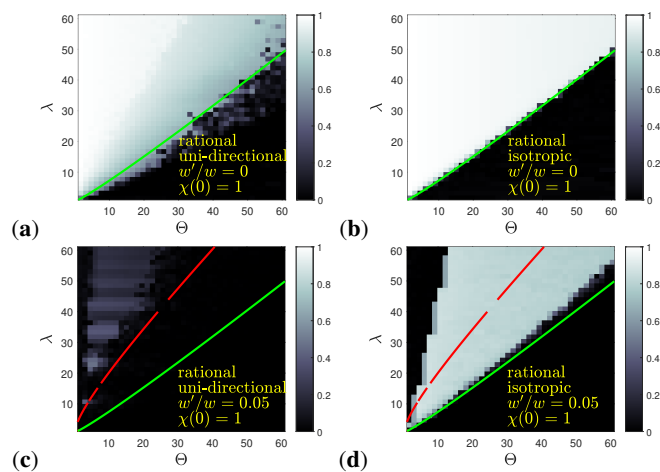


FIG. 12. Mass spread $\bar{\chi}$ as a function of λ and Θ for rational polygonal urns with $\alpha = \pi/3$, to be compared with the irrational ($\alpha = \pi/\sqrt{8}$) case of Fig. 7.

the number of velocity directions. Hence, the mechanism is not suitable to produce the uniformity of the velocity distribution. The behavior of $\bar{\chi}$ as a function of Θ/λ , for a rational rhomboidal urn with $\alpha = \pi/3$ is shown in panel (b) of Fig. 8, which evidences the sharpening of the transition region when N grows, with random initial velocities. Figure 15 shows the results of an analogous investigation for the peculiar rhomboidal urn with $\alpha = \pi/2$ (i.e. q is even). As in Fig. 12, simulations confirm that an (in fact remarkable) agreement with the theory is achieved only in presence of random initial velocities. Furthermore, as predicted by Eq. (8), the number of velocity directions, visible in Fig. 16 is less than with $\alpha = \pi/3$ (i.e. q odd). Another aspect which is worth highlighting is that, with $\alpha = \pi/2$, the bounce-back mechanism does not lead to a doubling of the velocity directions as previously noticed in Figs. 13 and 14 with $\alpha = \pi/3$.

V. CONCLUSIONS

In this work we studied the deterministic dynamics of N particles moving in a polygonal billiard table. We discussed the interplay of two important ingredients of the model: the bounce-back mechanism in the gates of the active channel and the geometry of the rhomboidal urns, which sensibly affects the ergodic properties of the dynamics. Our investigation of the steady state dynamics revealed that non-equilibrium phase transitions predicted by a stochastic theory may occur in the large N limit, as in the case of circular urns.^{26,27} The phase transitions are observed in the behavior of the stationary value of the observable $\bar{\chi}$, called mass spread, which may sharply switch from 0 (corresponding to a homogeneous state, in which the urns are equally crowded) to a value close to 1 (corresponding to an inhomogeneous regime with differently populated urns). The phase transition is triggered by the bounce-back mechanism, which kicks back the particles coming from an urn whenever their number in a gate exceeds a

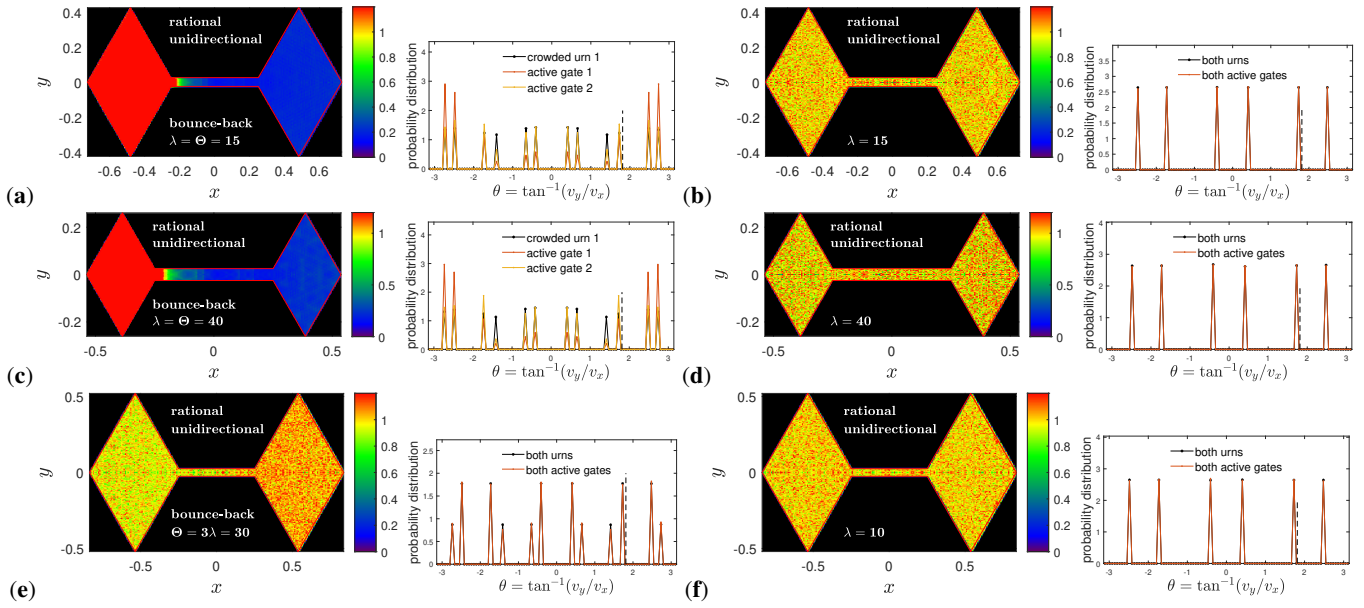


FIG. 13. Rational polygons with $\alpha = \pi/3$, connected by a single channel. All initial velocities have direction $\theta_0 = \pi/\sqrt{3}$. Systems **(a,c,e)** in presence and **(b,d,f)** in absence of the bounce-back mechanism. Each panel displays a stationary density plot and the corresponding stationary velocity histograms (θ_0 marked by vertical dashed line). **(a,b)** $\lambda = \Theta = 15$, **(c,d)** $\lambda = \Theta = 40$, and **(e,f)** $\lambda = 10$, $\Theta = 30$. Positions of the six spikes in **(b,d,f)** are in agreement with Eq. (7). The additional six spikes in **(a,c,e)** are due to the velocity reversal in the active channel, and agree with Eq. (9). Remaining parameters are: $w_a = 0.05$, $\ell_a = 0.5$, $\ell_p = 0.5$, $N = 10^3$ (same as in Fig. 6).

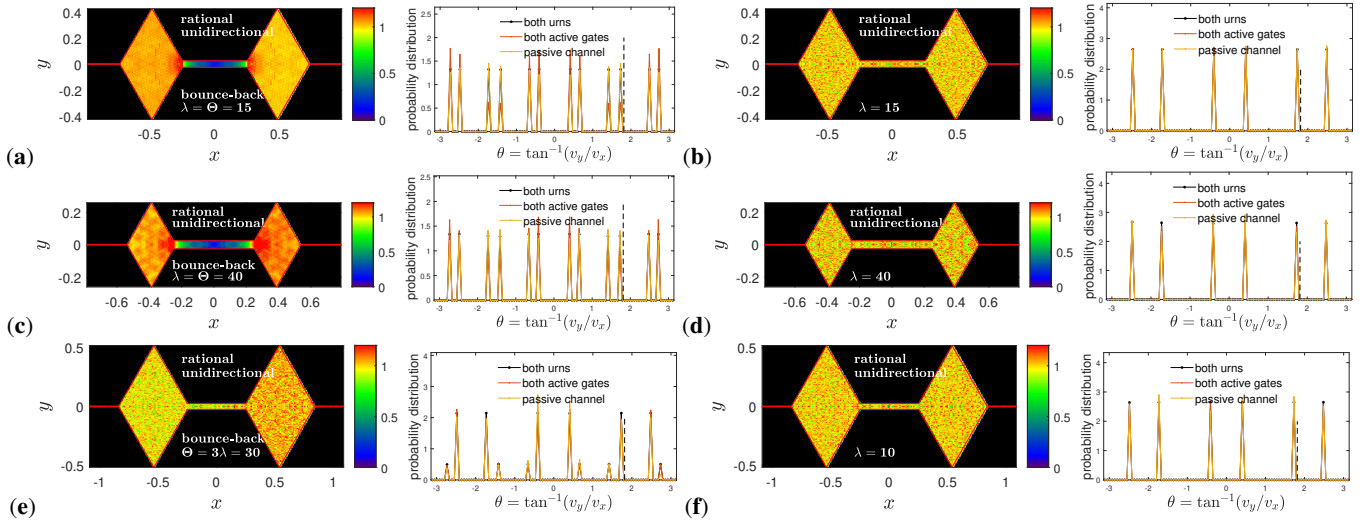


FIG. 14. Same geometry as in Fig. 13, where a passive channel with $w_p/w_a = 0.05$ and $\ell_p = 0.5$ has been added. All spikes agree with Eqs. (7) and (9).

threshold Θ . In absence of the aforementioned mechanism, particles are independent, and the only steady state is the one that occupies the largest fraction of phase space, *i.e.* the homogeneous state. To a certain extent, the perturbation introduced by the bounce-back mechanism in a gate reminds the action of a classical Maxwell demon. As this demon acts on particles coming from both urns, one can not foresee which of the two urns will eventually be crowded, if the initial state is $\chi(0) = 0$ and the parameters imply $\bar{\chi} = 1$.

The ergodic properties of the unperturbed dynamics consti-

tute another key ingredient in the onset of phase transitions, and in the application of the stochastic theory. Indeed, this theory predicts such transitions under the assumption that a uniform distribution of positions and velocities be realized. To make sense, this in turn requires large N , because there can be no uniform occupation of the positions and velocities spaces with a few particles. We have addressed, first, the study of irrational rhomboid-shaped urns, and proved that the corresponding dynamics is ergodic. Our simulations with large N not only confirmed the presence of the phase transition, but

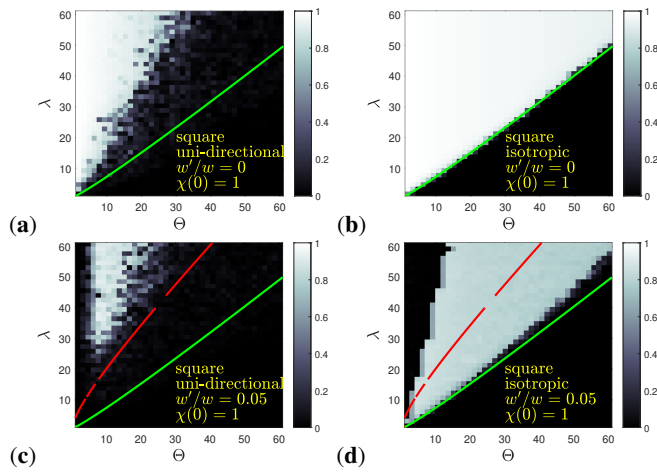


FIG. 15. Mass spread $\bar{\chi}$ as a function of λ and Θ for square urns ($\alpha = \pi/2$), for direct comparison with Fig. 7 (irrational polygons) and Fig. 12 (rational polygons, $\alpha = \pi/3$).

also that it is correctly described by the stochastic theory. With rational polygons, the picture changes. Depending on the geometry of the system (which may comprise, or exclude, the presence of the passive channel), our numerical simulations detected, in some cases, a phase transition, but the agreement with the theory turned out to be non-optimal. Moreover, this required the initial velocity distribution to be uniform, to beat the lack of ergodicity in rational urns, proved in Section II.

This clarifies the role of the various features of the microscopic dynamics in the description of collective phenomena, such as non-equilibrium phase transitions, and paves the way to further investigations, including the study of 3D billiard dynamics in presence of the bounce-back mechanism. It is worth stressing that, for insufficiently large N , our model correctly displays some peculiar features dictated by the microscopic dynamics and by the initial conditions, such as the migration in time from one state to another, among those predicted to be stable by the theory.

Unraveling connections with biological systems also offers promising scenarios. Indeed, the bounce-back mechanism exhibits an instance of a positive feedback control which is often observed in biology. One example is provided by the phenomenon of blood clotting: an injured tissue releases signal chemicals which activate platelets in the blood; the platelets, in turn, release a larger amount of chemicals, which activate more platelets, and so on. The foregoing process thus results in a cascade eventually leading to the formation of a blood clot.^{38–42} Another example of positive feedback loop comes from the Hodgkin cycle in membrane biology: the leakage of sodium ions through sodium channels, caused by the membrane of a nerve fibre, alters the membrane potential.^{43–47} This, in turn, causes a further opening of the channels, which leads to an increased flow of sodium ions. The process gives rise to a rapid increase of sodium leakage through the channels, which finally results in the generation of the nerve signal. The polygonal billiards considered in this work constitute models amenable to detailed analysis, that represent a first ap-

proximation to such important phenomena.

ACKNOWLEDGEMENTS.

LR acknowledges that this research has been partially funded by Ministero dell’Istruzione, dell’Università e della Ricerca (MIUR), Italy Grant No. E11G18000350001 “Dipartimenti di Eccellenza 2018–2022”. LR also acknowledges support from the Italian National Group of Mathematical Physics (GNFM) of INdAM.

DECLARATIONS

The authors have no conflicts to disclose.

Appendix A: Probabilistic Derivation of Stationary Currents

Here, we derive explicit formulae for the stationary currents in terms of geometrical and probabilistic arguments.^{26,27} Let A be the area of a rhomboidal urn, expressed by Eq. (10), in the case of two channels. Let $\rho(\mathbf{x}, \mathbf{v}) = 1/2\pi A$ denote the probability density for a particle with velocity $\mathbf{v} = (v\cos\theta, v\sin\theta)$ to be located at the point \mathbf{x} inside an urn, where $\theta \in [0, 2\pi]$, and the dimensionless speed $v > 0$ is fixed. Assume that the probability density is identical in the two urns.

Consider now a generic channel of width w and length ℓ connected to the urn. The assumed uniformity of the single-particle probability density, yields, via a geometrical argument, the typical number of particles that, in a small time interval of length $\delta > 0$, leave the i -th urn to enter the adjacent gate of width w and length $\ell/2$. Such a number reads:

$$2 \left(\frac{\bar{N}_i}{2\pi A} \right) w \int_0^{v\delta} \cos^{-1} \left(1 - \frac{x}{v\delta} \right) dx = \bar{N}_i \frac{wv\delta}{\pi A}, \quad (\text{A1})$$

where \bar{N}_i is the average number of particles residing in the i th urn. In Eq. (A1) we identify the quantity $wv\delta/\pi A$ with the probability p_δ that one particle in the urn enters the adjacent gate in the time interval δ .

Now, consider the typical time τ needed for a particle to cross a gate of length $\ell/2$, i.e.:

$$\tau = \frac{\pi\ell}{4v}, \quad (\text{A2})$$

which is computed from the knowledge of the length of the gate and the average horizontal component of particles velocity, $\langle v_x \rangle = 2v/\pi$.⁴⁸ The interval τ is then partitioned into smaller intervals of length δ . The probability that a number $s \ll \bar{N}_i$ of particles enter a gate from urn i in the time interval of length τ is

$$\binom{\bar{N}_i\tau/\delta}{s} p_\delta^s (1 - p_\delta)^{\bar{N}_i\tau/\delta - s}. \quad (\text{A3})$$

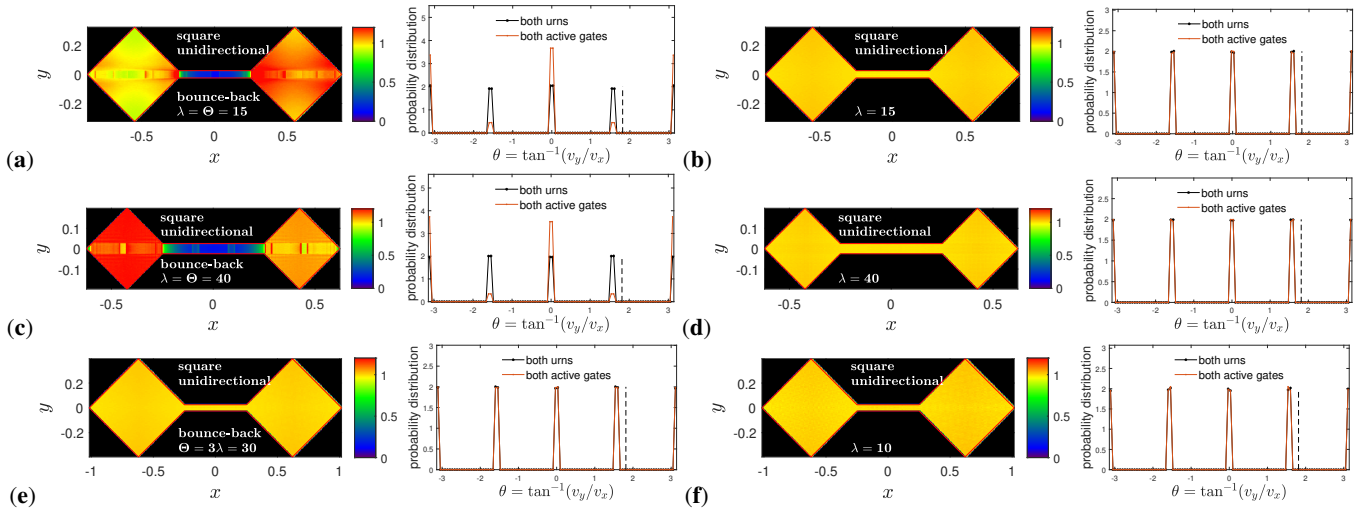


FIG. 16. Square urns ($\alpha = \pi/2$), connected by a single channel. All initial velocities have direction $\theta_0 = \pi/\sqrt{3}$. Each panel displays a stationary density plot and the corresponding stationary velocity histograms (θ_0 marked by vertical dashed line). In panels (a,c,e) the bounce-back mechanism is active; in panels (b,d,f) it is not. (a): $\lambda = \Theta = 15$; (b): λ like in (a). (c): $\lambda = \Theta = 40$; (d) λ like (c). (e): $\lambda = 10$, $\Theta = 30$; (f) λ like (e). Remaining parameters are: $w_a = 0.05$, $\ell_a = 0.5$, $\ell_p = 0.5$, $N = 10^3$ (same as in Fig. 6). The positions of the four spikes are in agreement with Eq. (8).

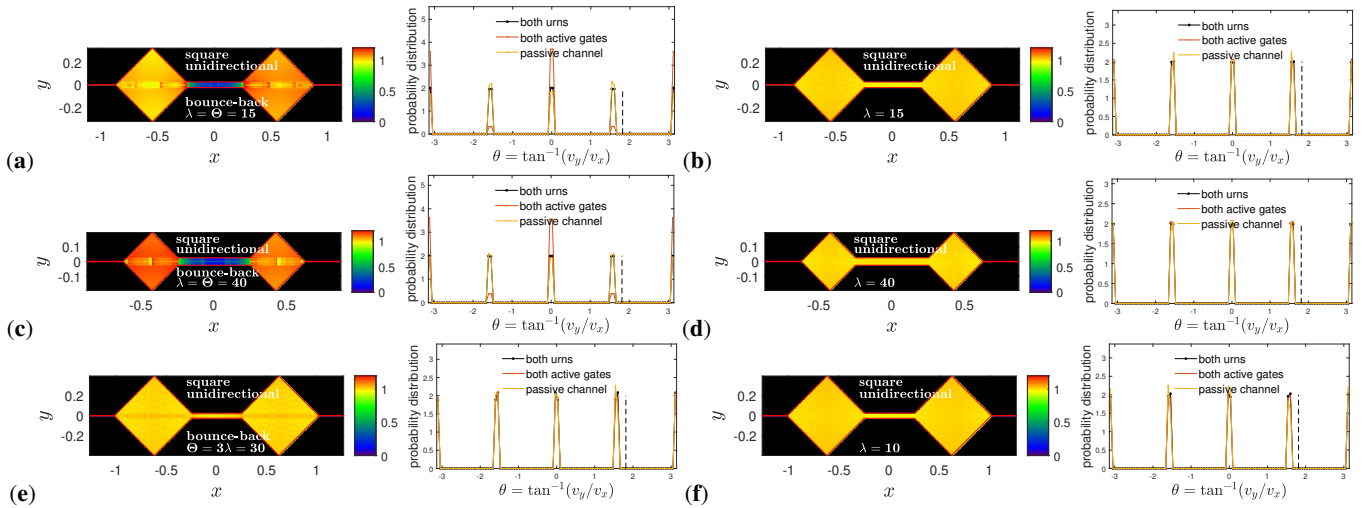


FIG. 17. Same as in Fig. 16 for the $\alpha = \pi/2$ rational polygons, plus a passive channel with $w_p/w_a = 0.05$ and $\ell_p = 0.5$. Spike positions in agreement with Eq. (8).

Since p_δ/δ does not depend on δ , the Poisson limit theorem, for small δ , implies that the probability (A3) is well approximated by $\lambda_i^s e^{-\lambda_i}/s!$ with

$$\lambda_i = \frac{p_\delta \tau \bar{N}_i}{\delta} = \bar{N}_i \frac{w\ell}{4A}. \quad (\text{A4})$$

The variable λ_i represents the typical number of particles which enter the gate adjacent to the i -th urn in the time interval τ .

The probability that at most Θ particles, with Θ small with respect to N , enter this gate adjacent to the i -th urn during the time interval of width τ is

$$P_\tau^{(i)}(\Theta) = \sum_{s=0}^{\Theta} \frac{\lambda_i^s}{s!} e^{-\lambda_i} = \frac{\Gamma(\Theta + 1, \lambda_i)}{\Gamma(\Theta + 1)}, \quad (\text{A5})$$

where we recall the definition of Euler's upper incomplete gamma function

$$\Gamma(\beta, \Lambda) := \int_{\Lambda}^{\infty} s^{\beta-1} e^{-s} ds \quad \Lambda > 0. \quad (\text{A6})$$

Let us now consider a larger time interval of width t , and let us partition it in small intervals of width τ . Typically, only in $P_\tau^{(i)} t/\tau$ intervals, out of the total t/τ , the particles entering the gate will not be affected by the type of channel, active versus passive. Therefore, the typical number of particles that cross the gate per unit time can be estimated as the typical number of particles that enter the gate in an interval of length

τ , multiplied times $P_\tau^{(i)}t/\tau$, i.e.,

$$\frac{1}{t} \frac{P_\tau^{(i)}t}{\tau} \frac{1}{P_\tau^{(i)}} \sum_{s=0}^{\Theta} s \frac{\lambda_i^s}{s!} e^{-\lambda_i} = \frac{\lambda_i}{\tau} P_\tau^{(i)} (\Theta - 1) = \frac{\lambda_i}{\tau} \frac{\Gamma(\Theta, \lambda_i)}{\Gamma(\Theta)}, \quad (\text{A7})$$

If, on the other hand, $\Theta > N$, the probability that at most Θ particles enter a gate adjacent to the i -th urn during the time interval of width τ is just unity, $P_\tau^{(i)}(\Theta) = 1$, and the typical number of particles that cross the gate in the time interval τ equals the typical number that has entered the gate in the same time interval from the i -th urn, which is λ_i . Hence, the current leaving the i -th urn into the channel reads λ_i/τ in that case.

These general considerations immediately lead to the expressions for the specific currents for the system with active and passive channels, with widths w_a and w_p . The dynamics in the active channel, divided in two gates, is driven by the bounce-back mechanism (if $\Theta < N$), while in the passive channel the particles always get through.

Upon replacing w , τ , λ_i , and ℓ in the above expressions by their counterparts indexed by subscripts p and a for the passive and active channels, c.f., Eqs. (12), (13), the specific average net currents \bar{J}_p and \bar{J}_a in the passive and active channels, accounting for particles leaving an urn and also for those coming from the other urn, are therefore given by

$$\bar{J}_p(t) = \frac{1}{N\tau_p} (\lambda_{2,p} - \lambda_{1,p}), \quad (\text{A8})$$

and

$$\bar{J}_a = \frac{1}{N\tau_a} \left[\frac{\lambda_{1,a}\Gamma(\Theta, \lambda_{1,a}) - \lambda_{2,a}\Gamma(\Theta, \lambda_{2,a})}{\Gamma(\Theta)} \right], \quad (\text{A9})$$

which concludes the derivation of Eqs. (14) and (15).

- ¹J.-P. Bouchaud and A. Georges, "Anomalous diffusion in disordered media: statistical mechanisms, models and physical applications," *Phys. Rep.* **195**, 127 (1990).
- ²K. H. Andersen, P. Castiglione, A. Mazzino, and A. Vulpiani, "Simple stochastic models showing strong anomalous diffusion," *Eur. Phys. J. B* **18**, 447–452 (2000).
- ³R. Metzler and J. Klafter, "The random walk's guide to anomalous diffusion: a fractional dynamics approach," *Phys. Rep.* **339**, 1 (2000).
- ⁴S. Havlin and D. Ben-Avraham, "Diffusion in disordered media," *Adv. Phys.* **51**, 187 (2002).
- ⁵G. M. Zaslavsky, "Chaos, fractional kinetics, and anomalous transport," *Phys. Rep.* **371**, 461 (2002).
- ⁶R. Artuso and G. Cristadoro, "Anomalous transport: A deterministic approach," *Phys. Rev. Lett.* **90**, 244101 (2003).
- ⁷O. G. Jepps and L. Rondoni, "Thermodynamics and complexity of simple transport phenomena," *J. Phys. A: Math. Gen.* **39**, 1311 (2006).
- ⁸R. Klages, G. Radons, and I. M. Sokolov, eds., *Anomalous Transport: Foundations and Applications* (Wiley-VCH, Weinheim, 2008).
- ⁹U. B. M. Marconi, A. Puglisi, L. Rondoni, and A. Vulpiani, "Fluctuation-Dissipation: Response Theory in Statistical Physics," *Phys. Rep.* **461**, 111–195 (2008).
- ¹⁰I. Bronstein, Y. Israel, E. Kepten, S. Mai, Y. Shav-Tal, E. Barkai, and Y. Garini, "Transient anomalous diffusion of telomeres in the nucleus of mammalian cells," *Phys. Rev. Lett.* **103**, 018102 (2009).
- ¹¹A. Igarashi, L. Rondoni, A. Botrugno, and M. Pizzi, "Nonlinear diffusion and transient osmosis," *Commun. Theor. Phys.* **56**, 352–366 (2011).
- ¹²I. M. Sokolov, "Models of anomalous diffusion in crowded environments," *Soft Matter* **8**, 9043 (2012).
- ¹³A. Vezzani, E. Barkai, and R. Burioni, "Microscopic dynamics in rare events: generalized Levy processes and the big jump principle," *Sci. Rep.* **10**, 2732 (2020).
- ¹⁴O. G. Jepps, C. Bianca, and L. Rondoni, "Onset of diffusive behavior in confined transport systems," *Chaos* **18**, 013127 (2008).
- ¹⁵P. S. Burada, P. Hänggi, F. M. Marchesoni, G. Schmid, and P. Talkner, "Diffusion in confined geometries," *ChemPhysChem* **10**, 45–54 (2009).
- ¹⁶E. N. M. Cirillo, M. Colangeli, and A. Di Francesco, "Residence time in one-dimensional random walks in presence of moving defects," *Prob. Eng. Mech.* **69**, 103260 (2022).
- ¹⁷T. Harayama, R. Klages, and P. Gaspard, "Deterministic diffusion in flower-shaped billiards," *Phys. Rev. E* **66**, 026211 (2002).
- ¹⁸M. Colangeli, A. De Masi, and E. Presutti, "Latent heat and the Fourier law," *Phys. Lett. A* **380**, 1710–1713 (2016).
- ¹⁹M. Colangeli, A. De Masi, and E. Presutti, "Microscopic models for uphill diffusion," *J. Phys. A* **50**, 435002 (2017).
- ²⁰M. Colangeli, A. De Masi, and E. Presutti, "Particle models with self-sustained current," *J. Stat. Phys.* **167**, 1081–1111 (2017).
- ²¹M. Colangeli, C. Giardina, C. Giberti, and C. Vernia, "Nonequilibrium two-dimensional Ising model with stationary uphill diffusion," *Phys. Rev. E* **97**, 030103 (2018).
- ²²D. Andreucci, E. N. M. Cirillo, M. Colangeli, and D. Gabrielli, "Fick and Fokker–Planck diffusion law in inhomogeneous media," *J. Stat. Phys.* **174**, 469–493 (2019).
- ²³E. N. M. Cirillo and M. Colangeli, "Stationary uphill currents in locally perturbed zero-range processes," *Phys. Rev. E* **96**, 052137 (2017).
- ²⁴E. N. M. Cirillo, M. Colangeli, and R. Dickman, "Uphill migration in coupled driven particle systems," *J. Stat. Mech.* , 073203 (2019).
- ²⁵J. Orchard, L. Rondoni, C. Mejía-Monasterio, and F. Frascoli, "Diffusion and escape from polygonal channels: extreme values and geometric effects," *J. Stat. Mech.* **073208** (2021).
- ²⁶E. N. M. Cirillo, M. Colangeli, A. Muntean, O. Richardson, and L. Rondoni, "Deterministic reversible model of non-equilibrium phase transitions and stochastic counterpart," *J. Phys. A* **53**, 305001 (2020).
- ²⁷E. N. M. Cirillo, M. Colangeli, O. Richardson, and L. Rondoni, "Deterministic model of battery, uphill currents, and nonequilibrium phase transitions," *Phys. Rev. E* **103**, 032119 (2021).
- ²⁸L. A. Bunimovich, "On the ergodic properties of nowhere dispersing billiards," *Comm. Math. Phys.* **65**, 295 (1979).
- ²⁹Y. B. Vorobets, "Ergodicity of billiards in polygons," *Sbornik Math.* **188**, 389 (1997).
- ³⁰E. Gutkin, "Billiards in polygons," *Physica D* **19**, 311–333 (1986).
- ³¹E. Gutkin, "Billiard dynamics: a survey with the emphasis on open problems," *Reg. chaotic dyn.* **8**, 1–13 (2003).
- ³²D. Alonso, A. Ruiz, and I. De Vega, "Polygonal billiards and transport: Diffusion and heat conduction," *Phys. Rev. E* **66**, 066131 (2002).
- ³³O. G. Jepps and L. Rondoni, "Thermodynamics and complexity of simple transport phenomena," *J. Phys. A* **39**, 1311 (2006).
- ³⁴D. P. Sanders and H. Larralde, "Occurrence of normal and anomalous diffusion in polygonal billiard channels," *Phys. Rev. E* **73** (2006).
- ³⁵O. G. Jepps, C. Bianca, and L. Rondoni, "Onset of diffusive behavior in confined transport systems," *Chaos* **18**, 013127 (2008).
- ³⁶L. Salari, L. Rondoni, C. Giberti, and R. Klages, "A simple non-chaotic map generating subdiffusive, diffusive, and superdiffusive dynamics," *Chaos* **25**, 073113 (2015).
- ³⁷J. Orchard, L. Rondoni, C. Mejía-Monasterio, and F. Frascoli, "Diffusion and escape from polygonal channels: extreme values and geometric effects," *J. Stat. Mech. Theory Exp.* **2021**, 073208 (2021).
- ³⁸A. C. Guyton, *Textbook of Medical Physiology (8th ed)* (W.B. Saunders, Philadelphia, 1991).
- ³⁹F. N. Buijs, L. Leon-Mercado, M. Guzman-Ruiz, N. N. Guerrero-Vargas, F. Romo-Nava, and R. M. Buijs, "The circadian system: A regulatory feedback network of periphery and brain," *Physiol.* **31**, 170–181 (2016).
- ⁴⁰T. A. Wang, Y. V. Yu, G. Govindaiah, X. Ye, L. Artinian, T. P. Coleman, J. V. Sweedler, C. L. Cox, and M. U. Gillette, "Circadian rhythm of redox state regulates excitability in suprachiasmatic nucleus neurons," *Science* **337**, 839–842 (2012).
- ⁴¹J. S. O'Neill and A. B. Reddy, "Circadian clocks in human red blood cells," *Nature* **469**, 498–U70 (2011).
- ⁴²L. Shearman, S. Sriram, D. Weaver, E. Maywood, I. Chaves, B. Zheng,

- K. Kume, C. Lee, G. van der Horst, M. Hastings, and S. Reppert, "Interacting molecular loops in the mammalian circadian clock," *Science* **288**, 1013–1019 (2000).
- ⁴³E. He, O. Kapuy, R. A. Oliveira, F. Uhlmann, J. J. Tyson, and B. Novak, "System-level feedbacks make the anaphase switch irreversible," *Proc. Natl. Acad. Sci. USA* **108**, 10016–10021 (2011).
- ⁴⁴I. Rybak, J. Paton, and J. Schwaber, "Modeling neural mechanisms for genesis of respiratory rhythm and pattern .2. network models of the central respiratory pattern generator," *J. Neurophysiol.* **77**, 2007–2026 (1997).
- ⁴⁵I. A. Rybak, N. A. Shevtsova, M. Lafreniere-Roula, and D. A. McCrea, "Modelling spinal circuitry involved in locomotor pattern generation: insights from deletions during fictive locomotion," *J. Physiol. - London* **577**, 617–639 (2006).
- ⁴⁶Y. Li, G. Schmid, P. Haeggi, and L. Schimansky-Geier, "Spontaneous spiking in an autaptic Hodgkin-Huxley setup," *Phys. Rev. E* **82** (2010).
- ⁴⁷Y. Xie, L. Chen, Y. M. Kang, and K. Aihara, "Controlling the onset of Hopf bifurcation in the Hodgkin-Huxley model," *Phys. Rev. E* **77** (2008).
- ⁴⁸The average horizontal component $\langle v_x \rangle$ of particles velocity inside the channels can be computed if their velocity directions inside the urns are uniformly distributed. In this case, the horizontal component $v_{x,k} = v \cos \theta_k$, $k = 1, 2, \dots, N$, is distributed as $v_x \sim \cos(\theta)$, where the angle of the k -th particle grows in the counter-clockwise direction. Consider particles entering a channel gate from the left to the right. To be able to enter the gate, the angle of their trajectory must be inside the interval $\theta \in (-\pi/2, \pi/2)$. Thus, the average horizontal component of their velocity will be computed as $\langle v_x \rangle = v \int_{-\pi/2}^{\pi/2} \cos(\theta) d\theta / \int_{-\pi/2}^{\pi/2} d\theta = 2v/\pi$.